

Predictive Maneuver Planning with Deep Reinforcement Learning (PMP-DRL) for comfortable and safe autonomous driving

Jayabrata Chowdhury, Vishruth Veerendranath, Suresh Sundaram, Narasimhan Sundararajan

Abstract—This paper presents a Predictive Maneuver Planning with Deep Reinforcement Learning (PMP-DRL) model for maneuver planning. Traditional rule-based maneuver planning approaches often have to improve their abilities to handle the variabilities of real-world driving scenarios. By learning from its experience, a Reinforcement Learning (RL)-based driving agent can adapt to changing driving conditions and improve its performance over time. Our proposed approach combines a predictive model and an RL agent to plan for comfortable and safe maneuvers. The predictive model is trained using historical driving data to predict the future positions of other surrounding vehicles. The surrounding vehicles' past and predicted future positions are embedded in context-aware grid maps. At the same time, the RL agent learns to make maneuvers based on this spatio-temporal context information. Performance evaluation of PMP-DRL has been carried out using simulated environments generated from publicly available NGSIM US101 and I80 datasets. The training sequence shows the continuous improvement in the driving experiences. It shows that proposed PMP-DRL can learn the trade-off between safety and comfortability. The decisions generated by the recent imitation learning-based model are compared with the proposed PMP-DRL for unseen scenarios. The results clearly show that PMP-DRL can handle complex real-world scenarios and make better comfortable and safe maneuver decisions than rule-based and imitative models.

Index Terms—Predictive planning, Autonomous Vehicle (AV), Spatio-temporal context, Reinforcement Learning, Imitation Learning

I. INTRODUCTION

INTELLIGENT Autonomous Vehicle (AV) development has advanced extraordinarily in recent years. However, autonomous driving on public roads still needs more work, especially in understanding the behaviors of surrounding traffic participants. To move safely and comfortably in dense traffic, an AV must understand the behaviors and intentions of its surrounding vehicles. One way to achieve this goal is a reliable vehicle communication system [1]. Using these communication channels, the AV can cooperate with other vehicles to decide its own actions. However, reliable communication can only be guaranteed sometimes. Another problem is that different vehicles have different communication protocols,

and communicating is really challenging. To avoid this problem, another way is to make the AV utilize both past and present contextual information to understand the behaviors of surrounding vehicles within its sensor range. Even in this approach, some critical problems could be solved. One of them is handling uncertainties in human behavior. Another problem is that other human drivers' decisions influence the behavior of the primary ego vehicle's behavior. In multi-agent scenarios, the future context of one ego vehicle also depends on the other surrounding vehicles' future trajectories. In the context of an ego vehicle, the predicted future trajectories of surrounding vehicles can infer these intentions. From these predictions, a safe region can be formulated where the ego vehicle can move. Hence, there is a need for a planning strategy for an ego vehicle incorporating a prediction module for surrounding vehicles in predictive maneuver planning algorithms. This planning algorithm should also handle unseen scenarios, which is the main contribution of this paper.

Earlier works in this area have used techniques like Imitation Learning (IL), Reinforcement Learning (RL) for motion planning for an AV. Before presenting our approach, a brief review of the above methods is given below. In IL-based work [2], a human-driven vehicle demonstration dataset has been used for learning the maneuver decision model. The learned driving model mimics a human driver's behavior. However, due to data distribution shifts from learning time, the IL model in [2] performed poorly in unknown scenarios like highly interactive lane change scenarios. In some work [3], Inverse Reinforcement Learning (IRL) has been used to learn human driving behavior. In [3], an IRL model Augmented Adversarial IRL (AugAIRL) was employed to change lanes in handcrafted highway scenarios. However, the absence of modeling uncertainties in the behaviors of surrounding vehicles in this paper represents a notable aspect with substantial implications for ensuring safety. Some models used open-source simulators like CARLA [4] and Vista [5] for end-to-end motion planning for autonomous vehicles. In [6], an imitative model has been trained to understand desirable behavior for an interpretable expert-like driving using data collected from the CARLA simulator. In [7] and [8], an imitation learning approach has been proposed for end-to-end autonomous driving. However, none of these models used trajectory predictions for evaluating behavior uncertainties. Recent works [9], [10], [11] use deep neural networks for trajectory predictions. These works model complex spatio-temporal relationships among the different vehicles. DST-CAN [12] has recently modeled the prediction

Jayabrata Chowdhury is with Robert Bosch Centre for Cyber-Physical Systems, Indian Institute of Science, Bangalore, India. Suresh Sundaram and Narasimhan Sundararajan are with the Artificial Intelligence and Robotics Lab, Dept. of Aerospace Engineering, Indian Institute of Science, Bangalore, India. Vishruth Veerendranath is with PES university, Bangalore, work done as a summer intern at Artificial Intelligence and Robotics Lab. Email: (jayabratac, vssuresh)@iisc.ac.in and (vishruthnath, ensundara)@gmail.com

Manuscript received May 23, 2023

uncertainties in a maneuver planning model. DST-CAN used an imitation model for interactive highway driving and showed the effectiveness of the use of a trajectory prediction module for safe maneuver planning for real-world scenarios using NGSIM I80 and US101 [13] datasets. However, since DST-CAN is an imitative model, it only tried to mimic some human behavior and suffered from scenarios where passenger comfort is also required along with safety.

An RL agent that learns through its own experience can overcome an imitative model's data distribution shift limitations. The works in [14], [15] used RL for learning neural network models to make maneuver decisions. These works use Bird's Eye View (BEV) raster image-based models for all the surrounding vehicles. This BEV representation has served as the input to the policy network. In some other works ([16], [17]), policy optimization methods were applied for lane-changing maneuvers. The work in [16] employs a Proximal Policy Optimization (PPO) [18] algorithm in a simulated environment for learning discrete lateral and longitudinal actions. In [17], a Soft Actor-Critic (SAC) [19] algorithm learns how to make steering and acceleration decisions in handcrafted traffic scenarios. In [20], [21], Deep Q Networks (DQNs) were used for lateral and longitudinal decisions. However, these works must incorporate the prediction module for surrounding vehicles to understand the future context and safe and comfortable decision-making. A detailed survey of RL-based autonomous driving can be found in [22]. Another concern is that RL learns in an active learning framework. Each time the RL agent interacts with the environment, it must collect new experiences to update the model. Getting real-world data during RL exploration may only be safe sometimes, as it can take dangerous actions. The surrounding traffic participants follow some hand-engineered rules in a closed simulation environment. The recent advancements in other fields of deep learning, like computer vision and natural language processing, have come from the help of vast and diverse real-world datasets. The RL algorithms can perform much better if some real-world datasets with interactions among vehicles are used for learning. Recent works [23], [24] focus on the importance of data-driven Offline Reinforcement Learning (ORL) frameworks. Based on the real-world data-based Vista simulator, [25] applied deep reinforcement learning to learn a policy to drive on unseen scenarios. However, this work omitted the incorporation of free space prediction and exclusively relied on the sparse reward to assess performance. An RL-based driving model with sparse reward could not learn to drive in a dense interactive scenario like a highway because there should be some signal to show how the RL agent performs every step. Hence, there is a need to develop a predictive maneuver planning algorithm with RL that can learn from real-world interaction and make both safe and comfortable decisions.

This paper proposes a new Predictive Maneuver Planning with Deep Reinforcement Learning (PMP-DRL) approach in AVs for safe and comfortable maneuver actions. The proposed approach assumes that a state-of-the-art perception module tracks other vehicles inside AV's sensor range and gives the positions of the vehicles. After observing the past positions, or the past trajectories, of the surrounding vehicles, a recurrent

Memory Neuron Network (MNN) [26], [27] predicts the future trajectories of those vehicles without any HD map, learning only with vehicle dynamics. These predicted trajectories of the surrounding vehicles are passed through a context generator. The context generator generates the input representation for spatio-temporal context-aware grid maps. The grid maps contain the past, present, and predicted future contextual information. The probabilistic occupancy grid maps encode future positions with prediction uncertainties. This work uses real-world driving interaction datasets for RL agents. NGSIM I80 and US-101 [13] datasets are used to learn and evaluate the learned RL agent. A simulation environment has been developed where surrounding vehicles move according to the trajectories given in the datasets. Some reward function designs for a dense reward function and network architecture tricks have been developed based on the dataset for better performance. The Double Deep Q Network (DDQN) [28] is employed to learn the hierarchical lateral and longitudinal decisions with the unicycle model for continuous decisions. The model was trained with high and low-congestion datasets and evaluated with the medium-congestion dataset as given in DST-CAN [12]. This paper gives importance to passenger comfort along with safety. Hence, the experiments are developed to find passenger comfort in the number of cases with jerkings and the safety of actions taken. The training sequence consistently improves average acceleration, passenger comfortability, and safety measures. The final comparative results show that our proposed PMP-DRL performs 51.79% and 51.20% better than the rule-based and baseline imitation-based model in unseen traffic scenarios. It has been found that there is a trade-off between safety and passenger comfort.

The paper is organized as given below. Section II describes the methodology for solving the problem of predictive motion planning with RL, details of action space, reward design, and architectural details. Section III details the simulation environment, metrics developed, and performance evaluation of PMP-DRL. Finally, the conclusions from the study are summarised in section IV.

II. PREDICTIVE MANEUVER PLANNING WITH DEEP REINFORCEMENT LEARNING (PMP-DRL)

This section describes the method to solve Predictive Maneuver Planning with Deep Reinforcement Learning (PMP-DRL) scheme. The approach uses Double Deep Q Network (DDQN) with context-aware grid maps processed by a Convolutional Neural Network (CNN). Before getting into the details of the architecture and training of the algorithm for PMP-DRL, the design of a context-aware grid-based observation space, action space design for comfort and safety analysis, and design of dense reward function are discussed.

A. Problem formulation

One of the biggest challenges in safe and comfortable driving on a public road is understanding the behavior of the ego AV's surrounding vehicles. If the surrounding vehicles' future poses can be predicted, then it is easier to understand their behavior. Fig. 1 shows the importance of predicting

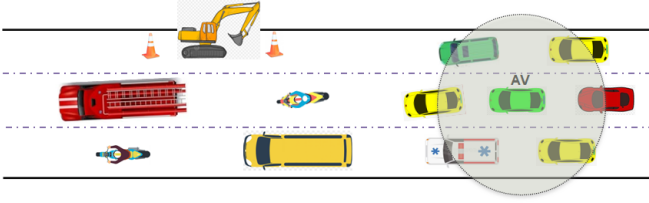


Fig. 1: A common traffic scenario with an AV in operation

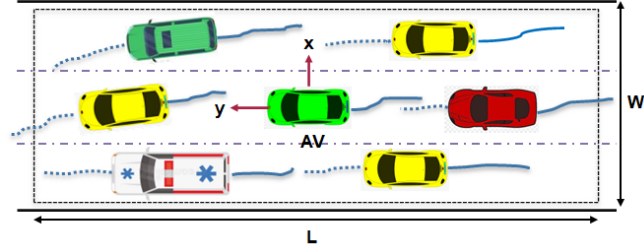


Fig. 2: A context region with an AV at the center

the future positions of the surrounding vehicles. The dotted circular line shows the AV's sensor range. Since the static obstacle is not in the sensor range of the AV, it cannot detect the reason for the traffic flow change. If surrounding vehicles' future positions can be predicted, it will be easier for the AV to understand how the driving scenario will evolve. AV can then decide on a safe and passenger-comfortable action depending on the predicted trajectories of surrounding vehicles. In recent work [20], Deep Reinforcement Learning (DRL) has been used for decision-making. This paper employs DRL for maneuver decision-making, incorporating a prediction module for safe and comfortable decisions.

B. Observation space for DRL

This paper presents a way to incorporate the spatio-temporal context information of an AV in an occupancy grid-based format without using High Definition map. We assume that HD map information is unavailable to an AV since building and maintaining a HD map is difficult. Also, HD map information processing is computationally heavy, and it may be noted that all sensors have their limitations. Hence, in this paper, context-aware grid maps are developed around the AV. These grid maps consist of occupancy maps for the present and past time frames and Probabilistic Occupancy Maps (POMs) with grid occupancy probabilities of surrounding vehicles. Depending on the AV's sensor range, a context region is chosen for making the context-aware grids, as shown in Fig.2. The context region assumes two adjacent lanes and a sensor range of 90 feet for the AV, as shown in Fig.2. \mathbf{P}_o and \mathbf{P}_e denote the past positions of the surrounding vehicles and the ego vehicle for p time frames. For Predictive Motion Planning (PMP), future positions of the surrounding vehicles' are predicted as $\hat{\mathbf{P}}_o$ for T future timesteps.

$$\begin{aligned} \{\mathbf{P}_e\} &= \{(x_a^{-p}, y_a^{-p}), (x_a^{-p+1}, y_a^{-p+1}), \dots, (x_a^0, y_a^0)\} \\ \{\mathbf{P}_o\} &= \{(x_{o_i}^{-p}, y_{o_i}^{-p}), (x_{o_i}^{-p+1}, y_{o_i}^{-p+1}), \dots, (x_{o_i}^0, y_{o_i}^0)\} \\ \{\hat{\mathbf{P}}_o\} &= \{(\hat{x}_{o_i}^1, \hat{y}_{o_i}^1), (\hat{x}_{o_i}^2, \hat{y}_{o_i}^2), \dots, (\hat{x}_{o_i}^T, \hat{y}_{o_i}^T)\} \end{aligned} \quad (1)$$

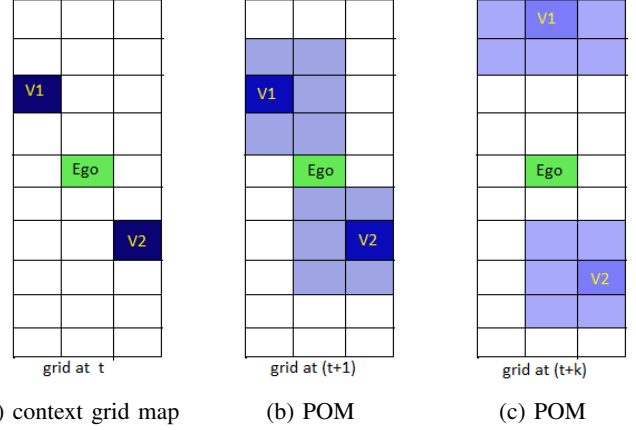


Fig. 3: Context and POM embedding for different time steps

where $i = 1, 2, \dots, N$; N is number of surrounding vehicles inside AV's sensor range. Here, we use a Memory Neuron Network (MNN) for the trajectory prediction of vehicles as described in [29]. We assume that HD map information is unavailable to an AV since building and maintaining an HD map is difficult. Also, HD map information processing is computationally heavy, and all sensors have limitations. Hence, the MNN is trained with Root Mean Squared Error (RMSE) loss function for trajectory prediction using only position information. MNN has been employed for multi-step prediction of future positions as given in the Eqns 2 and 3.

$$\bar{x}_{t+1} = x_t + \Delta \bar{x}_t; \quad \bar{y}_{t+1} = y_t + \Delta \bar{y}_t \quad (2)$$

$$\bar{x}_{t+(k+1)} = \bar{x}_{t+k} + \Delta \bar{x}_{t+k}; \quad \bar{y}_{t+(k+1)} = \bar{y}_{t+k} + \Delta \bar{y}_{t+k} \quad (3)$$

where $k = 1, 2, \dots, (T - 1)$. Occupancy grid maps are then created from the predicted positions of surrounding vehicles with respect to the distance from the ego vehicle. Since there are always uncertainties in predicting surrounding vehicles' future positions with increasing prediction horizons, it has been assumed here that a vehicle can be at any of the surrounding eight grids around the grid predicted by MNN. This assumption comes from the RMSE for different prediction horizons. The predicted grid by MNN is given an occupancy probability value as given in Equ. 4.

$$\mathbf{P}(t) = 0.47 + \sqrt{0.236 - 0.004t} \quad (4)$$

where $0 \leq t \leq 30$ is the time index. This study used 3 seconds of past trajectories to build context-aware grid maps as DST-CAN [12] showed that 3 seconds prediction horizon is good enough for planning. One occupancy grid map and POM are shown in Fig. 3. The final past occupancy maps and POMs are stacked to make a 3-dimensional context-aware occupancy grid map consisting of 60 channels of 13x3 dimensions. The occupancy grid map creation uses the same procedure as described in DST-CAN [12] and is given in Algo 1.

C. Action space

The PMP-DRL algorithm aims to generate safe, efficient, and comfortable maneuvering decisions from predicted trajectories of surrounding vehicles. The action space design takes

Algorithm 1 Context-aware grids generation pseudo code

- 1: **Inputs:** Past track history set $\{\mathbf{X}_h\}_{i=1}^{\mathcal{D}}$ where \mathcal{D} is the number of surrounding vehicles detected by the AV sensors, pre-trained weights for Memory Neuron Network (MNN), current time step t , prediction horizon T
- 2: **Initialize:** \mathcal{G} is a $13 \times 3 \times 60$ array of zeros
- 3: **Step 1:** Obtain the *context-aware grid* \mathcal{G} :
- 4: **for** $v \leftarrow 1$ to \mathcal{D} **do**
- 5: **for** $\tau \leftarrow t - 30$ to $t + T$ **do**
- 6: **if** $\tau \leq t$ **then**
- 7: $\mathcal{G}(i, j, \tau) = 1.0$, where (i, j) is the grid indices obtained using the relative position \mathbf{X}_h of vehicle v w.r.t ego vehicle's position at time τ .
- 8: **else**
- 9: $\mathcal{G}(i, j, \tau) = \mathbf{P}(\tau)$, where (i, j) is the grid indices obtained using the predicted position of vehicle v (from MNN), and $\mathbf{P}(\tau)$ is calculated using 4. $\mathcal{G}(i \pm 1, j \pm 1, \tau) = \mathcal{G}(i \pm 1, j, \tau) = \mathcal{G}(i, j \pm 1, \tau) = ((1 - \mathbf{P}(\tau))/8)$
- 10: **end if**
- 11: **end for**
- 12: **end for**

care of the ego vehicle passenger comfort. A sudden change in maneuver decisions is not desirable for passengers. Hence, action space should be defined in such a way that only whenever required, the ego vehicle brakes hardly or suddenly changes lanes. Hence, the following abstract-level discrete meta-actions *lateral maneuver* = [hard left, soft left, same lane, soft right, hard right] and *longitudinal maneuver* = [accelerate, cruise, decelerate, brake] are chosen to consider as the action space. This action space should reflect the comforts of passengers and the decisions like *braking* should be taken only when there is no way to prevent near-collision scenarios. If enough space is available in front of the ego vehicle, it should only slowly decelerate because it is comfortable for passengers. The discrete meta-actions are then converted to continuous action signals for taking a step in the driving environment. There is a fixed change in velocity and yaw angle for each action. Since accurately predicting the bicycle model parameters are difficult with vision sensors' limitations, the ego vehicle uses a unicycle model as given in Equ. 5.

$$\dot{x}_t = v_t * \sin \phi_t; \dot{y}_t = v_t * \cos \phi_t; \dot{\phi}_t = \Delta \phi_t \quad (5)$$

where x_t, y_t, ϕ_t are the positions and yaw angle of the ego vehicle. v_t is the velocity of the ego vehicle at the current time instant. The discrete lateral actions have been converted to continuous changes in the ego vehicle's yaw angles $\Delta \phi_t$. Similarly, longitudinal actions are converted to changes in the ego vehicle's velocity Δv_t .

$$\begin{aligned} v_t^x &= (x_t - x_{t-1})/\Delta t; v_t^y = (y_t - y_{t-1})/\Delta t \\ v_t &= \sqrt{(v_t^x)^2 + (v_t^y)^2}; \phi_t = \tan^{-1}(x_t - x_{t-1}/y_t - y_{t-1}) \\ v_{up} &= v_t + \Delta v_t; \phi_{up} = \phi_t + \Delta \phi_t \\ x_{t+1} &= x_t + (v_{up} \sin \phi_{up} \Delta t); y_{t+1} = y_t + (v_{up} \cos \phi_{up} \Delta t) \end{aligned} \quad (6)$$

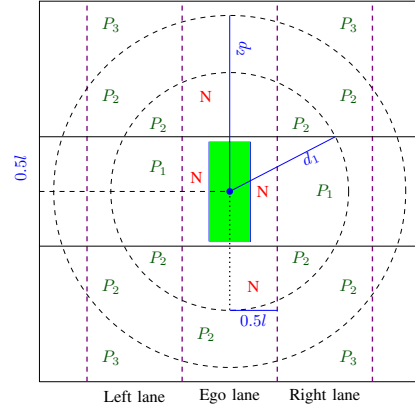


Fig. 4: Positive and negative reward region for AV

Since the action space is discrete, the discrete actions are converted to a change in control action $u_t = [\Delta v_t, \Delta \phi_t]$ for updating the position of ego vehicle with the unicycle model. In Equ. 6, x_t, y_t are positions of the ego vehicle at the current time instant. x_{t-1}, y_{t-1} are position of ego vehicle at previous time instant. Δt is the time interval. In this work, $\Delta t = 0.1$ seconds. In Equ. 6, at first current instant velocity v_t and yaw angle ϕ_t are calculated. Next, velocity and yaw angle is updated to get new velocity v_{up} and yaw angle ϕ_{up} . Equ 6 then calculates the next position of the ego vehicle.

D. Reward function

The reward function is a crucial component of DRL algorithms. Generally, a positive reward is given if an AV reaches its goal. However, training a DDQN with this kind of sparse reward is difficult. Hence, the reward has been modified using distance-based, imitation-based, and off-road components. One component is a distance-based reward for preventing near-collision scenarios. The second part is a reward for imitation learning based on human driving behavior. The third and last part is an off-road reward for preventing the ego vehicle from taking an action that can go out of the road boundary. These three components are then combined to contribute to the final reward for an action. The safe region around the ego vehicle is defined based on the average length ($l = 15 \text{ foot} \approx 4.57 \text{ m}$) and width (w) of vehicles on the road given in the dataset. If any vehicle comes near the ego vehicle laterally, a negative reward is given for that action. If any surrounding vehicle is within distance d_1 of the ego vehicle on the front and backside, there is a risk of collision. Hence, this region is a negative reward region. The ego vehicle is at the center, shown in green in Fig.4. The positive and negative reward regions have been shown in Fig.4 with "P" and "N." The positive reward region is divided into three parts, as shown in Fig. 4. If a vehicle is moving in the same direction parallelly to the ego vehicle, maintaining a safe distance (within distance $d_1 = (l + 1) \text{ foot} = 16 \text{ foot} \approx 4.88 \text{ m}$), then that region is denoted as positive region P_1 . If a vehicle is not very close to the ego vehicle (within distance $d_2 = (1.5l + 2.5) \text{ foot} = 25 \text{ foot} \approx 7.62 \text{ m}$), then it is in the positive reward region P_2 . If any vehicle is more than d_2 distance from the ego

Algorithm 2 Details of Reward function

1: **Input:** Predicted future position (ego_x^{pr} , ego_y^{pr}) of ego vehicle for action, actual ego vehicle position (ego_x^{ac} , ego_y^{ac}) in future extracted from dataset, surrounding vehicles' future positions (s_x^i , s_y^i) where $i = 1, 2, \dots, S$; S is number of surrounding vehicles in sensor range.

2: **Output:** Total reward for an action

3: **Initialize:** $p_1 = 0, p_2 = 0, p_3 = 0, p_{count} = 0, n_{count} = 0, r_{dis} = 0, r_{pos} = 0, r_{neg} = 0, r_{imit} = 0, r_{off-road} = 0, reward = 0, c_1 = 5, c_2 = 125, k_1 = 2, k_2 = -6$

4: **Part 1:** Distance based reward

5: **for** $i \leftarrow 1$ to S **do**

6: $\Delta x = ego_x^{pr} - s_x^i; \Delta y = ego_y^{pr} - s_y^i; d = \frac{\Delta x}{\sqrt{(\Delta x)^2 + (\Delta y)^2}}$

7: **if** $|\Delta y| \leq 0.5l$ **then**

8: **if** $|\Delta x| \geq 0.5l$ **then**

9: $p_1 \leftarrow p_1 + 1; p_{count} \leftarrow p_{count} + 1$

10: **if** $p_1 \leq 1$ **then**

11: $r_{pos} = r_{pos} + c_1 \tanh(|\Delta x| - 0.5l)$

12: **end if**

13: **else**

14: $n_{count} = n_{count} + 1$

15: $r_{neg} = r_{neg} + c_1 \tanh(|\Delta x| - 0.5l)$

16: **end if**

17: **else**

18: **if** $d \leq d_1$ and $|\Delta x| \leq 0.5l$ **then**

19: $n_{count} = n_{count} + 1$

20: $r_{neg} = r_{neg} + c_1 \tanh(d - d_1)$

21: **else if** $d \leq d_2$ **then**

22: $p_2 \leftarrow p_2 + 1; p_{count} \leftarrow p_{count} + 1$

23: $r_{pos} = r_{pos} + (d/c_1)$

24: **else**

25: $p_3 \leftarrow p_3 + 1; p_{count} \leftarrow p_{count} + 1$

26: $r_{pos} = r_{pos} + (c_2/d)$

27: **end if**

28: **end if**

29: **end for**

30: $r_{dis} = r_{dis} + (r_{pos}/p_{count}) + k_1 r_{neg}$

31: **Part 2:** Imitation based reward

32: $x_{err} = ego_x^{pr} - ego_x^{ac}; y_{err} = ego_y^{pr} - ego_y^{ac}$

33: $imit_{err} = 0.25|x_{err}| + 0.1|y_{err}|; r_{imit} = -0.5(imit_{err})$

34: **Part 3:** Off-road reward

35: **if** $ego_x^{pr} \leq 0$ or $ego_x^{pr} \geq (\#lane * lane\ width)$ **then** $r_{off-road} = k_2$

36: $reward = r_{dis} + r_{imit} + r_{off-road}$

vehicle, then that region is a positive reward region P_3 . The number of surrounding vehicles in each region is calculated as p_1, p_2, p_3, n_{count} to define the final distance-based reward. The reward is designed for a smooth transition from one region to another. The reward is then scaled so that vehicle in a near-collision scenario gets higher importance. The imitation part of the reward is calculated by the distance of the ego vehicle from the position of human decisions. The imitation part of the reward is scaled according to the x, y position displacement error. The reward design details are given in Algo.2.

E. Architecture and training details

The architecture of the proposed PMP-DRL method is shown in Fig.5. A simulation environment has been developed based on a real-world NGSIM dataset. At every time step, the simulation environment will reward the ego vehicle and provide observation containing information about the positions of surrounding vehicles inside the ego vehicle's sensor range. Next, the context-generator block processes the past trajectories and provides context-aware grid maps and POMs. The action engine shown in the Fig.5 has been trained in two different ways. At first, an imitation model is learned, then a DDQN model is trained. The imitative model has two parts. The first part consists of spatio-temporal information extraction with a Convolutional Neural Network (CNN), and the second part is a decision neural network. We first train an imitative model for maneuver decisions similar to that given in the DST-CAN [12]. The imitative model is trained with rule-based decisions. The imitative model first uses a CNN to encode the context-aware social grid maps to a fixed-size state encoding. The CNN uses two three-dimensional convolutional layers. This encoded state is then passed through two different fully connected decision head layers. These decision head layers output lateral and longitudinal decisions. The imitative model is trained with binary cross entropy loss as given in Eq.7.

$$\mathcal{L} = -\frac{1}{N} \sum_{i=1}^N y_i \log(p(y_i)) + (1 - y_i) \log(1 - p(y_i)) \quad (7)$$

where y_i is the rule based decision and $p(y_i)$ is the predicted decision. N is the total number of samples. For learning this model, NGSIM US101 and I80 datasets are employed. Each vehicle's lateral and longitudinal actions are extracted from these datasets. Learning imitative models with a highly imbalanced dataset is very difficult. Learning a good driving model with an imbalanced long-tail dataset like NGSIM is very challenging. Table I shows how the different driving decisions are distributed according to traffic rules. At first, all the data are used for the first training epoch. For some input spatio-temporal grid maps, the imitation network decides the same as rule-based decisions. Those spatio-temporal grid maps are removed from training data for imitation learning. Since most of the dataset comprises cruising on the same lane, a unique data pruning method has been employed for training. Hence, only a tiny portion (20%) of cruise maneuvers are taken for training the imitative model after the data pruning process. After training the imitative model, we want to learn how the DDQN-based decision algorithm works for different scenarios. For training the DDQN model, two Q networks (primary network Q_θ and target network $Q_{\theta'}$) are used during training. The Q network has been trained for different driving datasets sequentially. The input datasets come sequentially from low-density (ld) and high-density (hd) datasets for training the Q network. For scenarios where rule-based decisions are cruising, only 50% of those transitions (s_t, a_t, r_t, s_{t+1}) are stored in the replay buffer. For other rule-based decisions, all transitions are stored in the replay buffer. The same trained CNN for the imitative model has been used for state encoding

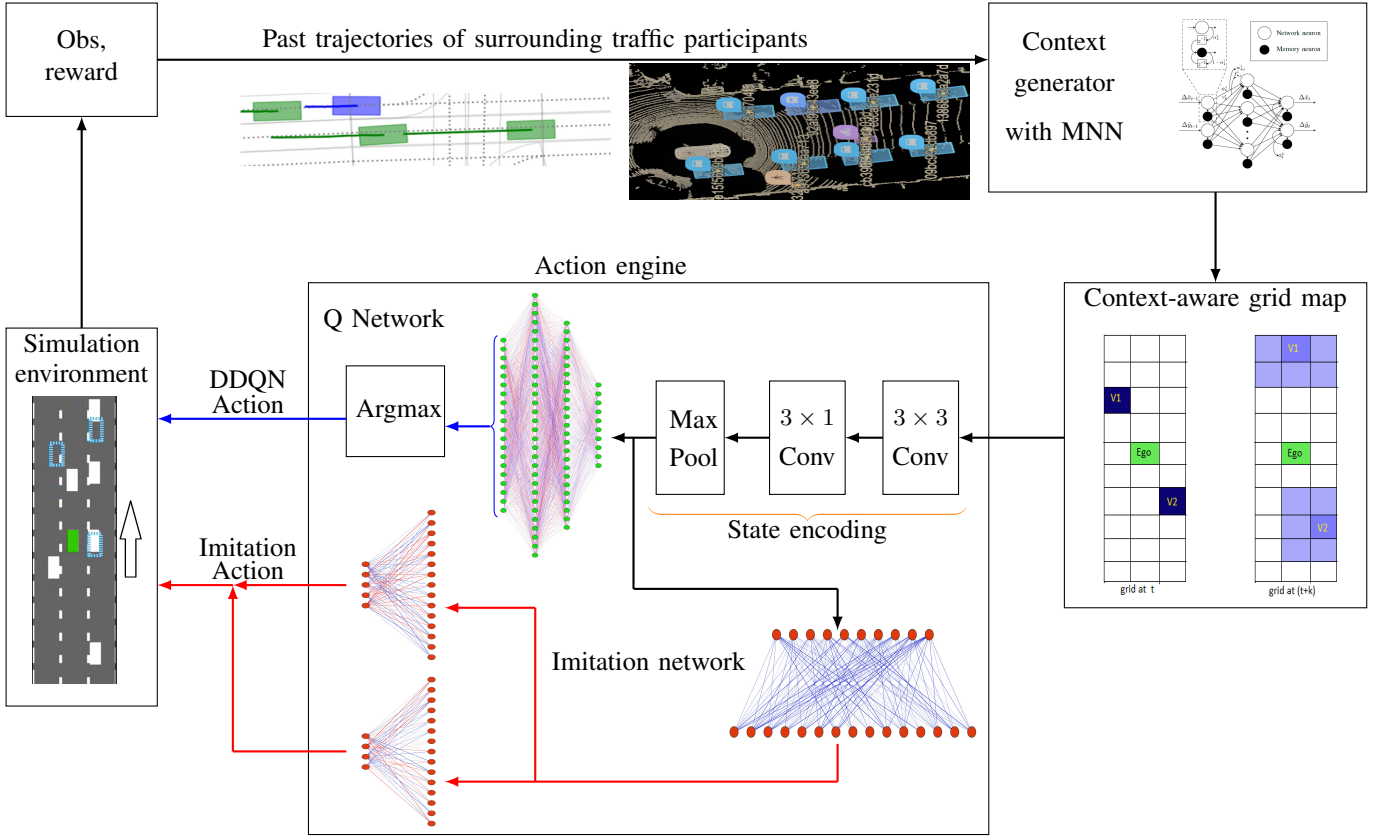


Fig. 5: Architecture for PMP-DRL

	US101 07:50-08:05	US101 08:05-08:20	US101 08:20-08:35
Follow same lane	90.45%	90.51%	90.78%
Hard left	0.26%	0.27%	0.18%
Soft left	4.13%	4.13%	4.24%
Hard right	0.12%	0.20%	0.19%
Soft right	5.04%	4.89%	4.60%
Accelerate	13.65%	14.37%	15.44%
Brake	0.36%	0.75%	0.84%
Cruise	79.79%	77.18%	75.36%
Decelerate	6.20%	7.70%	8.35%
Same lane & cruise	70.62%	68%	66.52%
Total samples	1180598	1403095	1515240

	I80 16:00-16:15	I80 17:00-17:15	I80 17:15-17:30
Follow same lane	90.55%	91.82%	92.34%
Hard left	0.14%	0.37%	0.52%
Soft left	3.20%	2.69%	2.36%
Hard right	0.47%	1.04%	1.26%
Soft right	5.64%	4.08%	3.53%
Accelerate	14.43%	14.65%	14.88%
Brake	0.80%	2.73%	3.82%
Cruise	75.64%	72.36%	70.97%
Decelerate	9.13%	10.26%	10.33%
Same lane & cruise	66.79%	65.59%	65.09%
Total samples	1262678	1549918	1753791

TABLE I: Details of NGSIM traffic dataset

for PMP-DRL. DDQN has been used for action selection. After the state encoding by CNN, three fully connected neural network layers are used for the decision head. The DDQN is trained with the Huber loss function. The final fully connected

layer gives the Q values for different decisions. The decision with the highest Q value is taken for an action. Algo. 3 describes the training procedure of the imitative and offline data-driven reinforcement learning-based models in detail.

III. PERFORMANCE EVALUATION OF PMP-DRL

This section presents the performance evaluation of the proposed PMP-DRL method based on real-world NGSIM I80 and US101 [13] datasets. The simulation setup is described first, then performance evaluation metrics are described. PMP-DRL's performance is compared with the rule-based method and recent baseline imitative model DST-CAN [12]. Finally, ablation studies have been conducted to gain insight into the importance of predictive modules with past context encoding and reward design components, and study results are presented to indicate the effectiveness of the prediction module.

A. RL Simulation setup

A simulation environment had to be developed where surrounding vehicles show human driving behaviors. This kind of environment can capture real-world mixed autonomous-human driving interactions. If surrounding vehicles follow some hand-coded rules, then autonomous ego vehicles cannot understand human behaviors. Hence, an OpenAI Gym environment has been created based on the actual human-driving NGSIM I-80 and US-101 datasets. The datasets consist of low, medium, and highly congested traffic scenarios. The vehicle trajectories

Algorithm 3 Imitative and PMP-DRL training pseudo code

```

1: Part 1: Imitative model training
2: Input: Context-Aware Spatio Temporal Grids as tensors
   with rule-based maneuver decisions
3: Initialize: CNN with the final output of the maneuver
   action classes and a blank list  $\mathcal{L}$  for storing tensor indices,
   initialize cruise count for data pruning  $k_{cruise} = 0$ 
4: Step 1: Pass all tensors through model for 1st epoch
5: for  $i \leftarrow 1$  to (Total number of social tensors) do
6:   if predicted action = actual action then
7:     Save the tensor index  $i$  to the list  $\mathcal{L}$ 
8:   end if
9: end for
10: Step 2: Remove the tensors in list  $\mathcal{L}$  from training dataset
   and get new training dataset with remaining data
11: Step 3: Train imitative model with new training dataset
12: for  $i \leftarrow 1$  to  $\mathcal{E}$  number of epochs do
13:   for  $j \leftarrow 1$  to (batch size  $b$ ) do
14:     if rule-based lateral action = cruise and
        $k_{cruise} \% 5 = 0$  then
15:        $k_{cruise} \leftarrow k_{cruise} + 1$  and go to line 19
16:     else
17:       Go to line 19
18:     end if
19:     Predict the maneuver action classes as probabili-
       ties and calculate the Binary Cross Entropy (BCE)
       loss  $\mathcal{L}$  as given in 7
20:   end for
21:   Back propagate gradients to learn weights
22: end for
23: Part 2: RL training
24: Initialize: Load the pre-trained CNN from the imitative
   model for state encoding and fix CNN weights. Initialize
   primary network  $Q_\theta$  and target network  $Q_{\theta'}$ .
25: for dataset in  $[US101_{ld}, I80_{hd}, I80_{ld}, US101_{hd}]$  do
26:   Initialize Replay Buffer  $\mathcal{B}$ ;  $k_{cruise} = 0$ 
27:   for  $veh \leftarrow 1$  to (vehicles available in dataset) do
28:     With probability  $\epsilon$ , choose  $a_t$  randomly,
29:     else choose  $a_t = \operatorname{argmax}_{a' \in \mathcal{A}} Q(s_t, a')$ 
30:     Take action  $a_t$  and get  $s_{t+1}, r_t$  from environment
31:     if rule-based lateral action = cruise then
32:        $k_{cruise} \leftarrow k_{cruise} + 1$ 
33:       if  $k_{cruise} \% 2 = 0$  then
34:         store  $(s_t, a_t, r_t, s_{t+1})$  in  $\mathcal{B}$ 
35:       end if
36:     else
37:       store  $(s_t, a_t, r_t, s_{t+1})$  in  $\mathcal{B}$ 
38:     end if
39:   end for
40:   for each update step do
41:     sample  $e_t = (s_t, a_t, r_t, s_{t+1})$  from  $\mathcal{B}$ 
42:      $Q^*(s_t, a_t) \approx r_t +$ 
        $\gamma Q_\theta(s_{t+1}, \operatorname{argmax}_{a'} Q_{\theta'}(s_{t+1}, a'))$ 
43:     Perform gradient step on  $(Q^*(s_t, a_t) - Q_\theta(s_t, a_t))^2$ 
44:   end for
45:   Update target network  $Q_{\theta'}$  parameters
46: end for

```

in the datasets are recorded at two different locations at different times of the day. The datasets comprise many traffic scenarios in the study regions, including on-ramps and off-ramps. These different scenarios include significant changes in traffic patterns. Since NGSIM is a real-world dataset, it also has the actual maneuver decisions taken by human drivers. Generally, a vehicle changes lanes within 8 to 10 seconds, as reported in [30]. Hence, we consider lane-changing action if a vehicle's lane id changes from the previous 4 seconds to the next 4 seconds. A braking decision is assumed if a vehicle's average speed over the next 5 seconds is lower than 0.8 times the current speed. The environment is designed so that the algorithm controls only one vehicle. Other surrounding vehicles follow the trajectories given in the dataset. One episode is defined for every vehicle's trajectory in the dataset. The low (ld) and highly (hd) congested traffic datasets are used for training the algorithm. After training, the algorithm is tested based on the dataset's unseen medium congestion traffic scenarios.

B. Performance Evaluation Metrics

The performance of an autonomous vehicle algorithm is evaluated based on its ability to decide on a safe and comfortable action. The evaluation methodology involves examining the anticipated outcomes of the present action within a short-term horizon. Specifically, the projected position of the ego vehicle after 0.1 seconds is computed based on the currently selected action. The algorithm's performance evaluation encompasses considerations of both safety and passenger comfort. The algorithm's performance is evaluated based on the following metrics:

- *Average acceleration:* This metric is derived by computing the mean value of the ego vehicle's acceleration. It serves as a measure of the ego vehicle's ability to navigate traffic scenarios with speed and fluidity. A higher metric value indicates a greater capacity for the vehicle to achieve accelerated movement within the traffic environment.
- *Percentage of uncomfortable scenarios:* Passenger comfort is an important measure to evaluate the performance of an autonomous vehicle. To evaluate passenger comfort, we can use the number of times a passenger experiences a jerk. Jerk is a measure of how quickly the vehicle's acceleration changes. There will be no jerk if the algorithm decides on an action that changes smoothly (like accelerating to cruising). However, there will be a jerk if the algorithm decides on an action that changes for more than one smooth change (like accelerating to braking). Jerk is calculated by dividing the number of times the algorithm's action changes for more than one smooth change by the total number of steps. The lower the jerk metric, the better the passenger comfort. Minimizing jerk can improve passenger comfort and make autonomous vehicles more enjoyable.
- *Percentage near collision scenarios:* This metric leverages the projected position of the ego vehicle, considering a prediction horizon of 0.1 seconds. It identifies

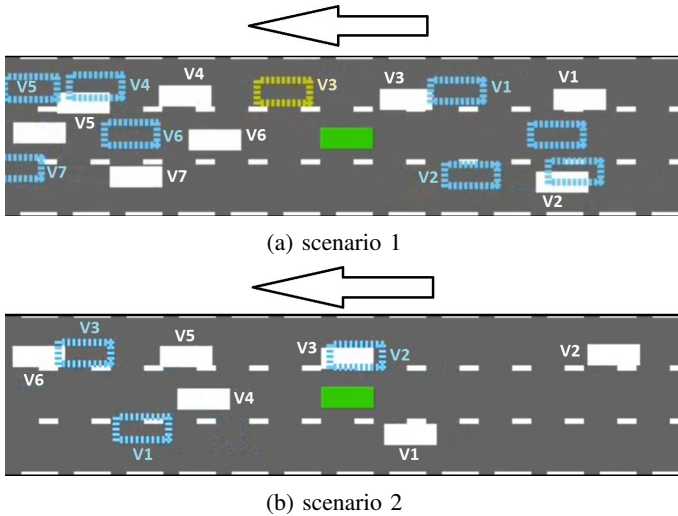


Fig. 6: Different driving scenarios

instances where any surrounding vehicle encroaches upon the proximity range associated with near-collision events, as specified in the reward design. These occurrences are tallied as near-collision scenarios, and the average frequency of such events is documented. A lower value of this metric is deemed advantageous, indicative of a reduced incidence of near-collision situations.

Two scenarios are shown in Fig.6. The ego vehicle is shown in green. Other surrounding vehicles in the context region of the ego vehicle are shown in white. The near future positions of other surrounding vehicles are given in dotted boxes. The blue dotted boxes are for those surrounding vehicles' future positions that will be at a safe distance from the ego vehicle. Yellow dotted boxes show the vehicles that will be near the ego vehicle. A typical scenario where vehicles V_2, V_4, V_5, V_6 are slowing down, is shown in Fig.6a. Vehicle V_7 is changing to the right lane in Fig.6a. Another scenario where vehicle V_1 is changing to the right lane is shown in Fig.6b.

C. Performance evaluation

The metrics defined above are used to evaluate the proposed PMP-DRL method's performance. Since some standard traffic rules are already available for driving, rule-based decisions are also considered for comparison. Also, this study tries to find the effectiveness of the self-learning strategy of data-driven reinforcement learning for autonomous driving. For this purpose, the PMP-DRL results have also been compared with a recent imitative model [12] based driving. The imitative model was trained using a supervised maneuver classification learning manner. This imitative model also uses the advantages of surrounding vehicles' future position prediction for decision planning. In this study, we have changed the action space of DST-CAN [12] to match our defined action space. We similarly trained the imitative model with rule-based decisions as ground truth decisions. The training and testing dataset setup has different data distributions of vehicle velocities, as shown in Table II. Consensus and conflict scenarios are evaluated separately for a comparison with the imitative model.

Vehicle velocity (m/s)	US101 07:50-08:05	US101 08:05:08:20	US101 08:20-08:35
Mean	4.827	8.939	7.836
Standard deviation	3.623	4.089	3.672
25 percentile	9.114	6.096	5.093
50 percentile	11.963	9.153	8.035
75 percentile	14.438	12.168	10.638

Vehicle velocity (m/s)	I80 16:00-16:15	I80 17:00-17:15	I80 17:15-17:30
Mean	7.722	5.622	4.827
Standard deviation	4.061	3.889	3.623
25 percentile	5.624	2.844	2.033
50 percentile	7.483	4.877	4.234
75 percentile	9.345	7.620	6.870

TABLE II: Details of vehicle velocities for NGSIM dataset

	Average acceleration (m/s^2)	Uncomfortable scenarios (%)	Near collision (%)
Consensus cases			
US101 (7:50-08:05)	0.314	37.349	11.812
I80 (17:15-17:30)	0.229	37.532	7.538
I80 (16:00-16:15)	0.267	37.508	8.697
US101 (08:20-08:35)	0.269	37.474	7.991
Conflict cases			
US101 (7:50-08:05)	0.311	37.675	19.019
I80 (17:15-17:30)	0.242	37.514	16.445
I80 (16:00-16:15)	0.267	37.508	8.697
US101 (08:20-08:35)	0.271	37.354	13.931

TABLE III: PMP-DRL performance during training sequence

Consensus cases are those where human decisions and rule-based decisions are the same. The PMP-DRL method has been trained in a sequence of datasets described in Algo. 3. After each training dataset, the performance has been evaluated and shown in Table III. From Table III, it can be found that the driving performance improved for all metrics sequentially. In the beginning, the average acceleration is high ($0.314m/s^2$ and $0.311m/s^2$, for consensus and conflict cases, respectively). However, the near-collision scenarios are also high initially (11.812% and 19.019% for consensus and conflict cases, respectively). Also, it can be found that there exists a trade-off between uncomfortable scenarios and near-collision scenarios. From these results, it can be concluded that PMP-DRL can understand driving scenarios better and learn to improve all the metrics. Before presenting the comparative results, we found how many near-collision scenarios are inside the NGSIM dataset according to the near-collision region around the ego vehicle described in the reward structure. The details are shown in Table IV. Table V shows the results of comparing different methods. This table has three results for traffic rule-based (Rule based), PMP with imitation learning (Imitation), and PMP with Deep Reinforcement Learning (PMP-DRL). It shows that the proposed PMP-DRL method performs much better than the other imitative and rule-based

	Consensus cases (%)		Conflict cases (%)	
	180	US101	180	US101
	17:00-17:15	08:05-08:20	17:00-17:15	08:05-08:20
Near collision scenarios	7.312 %	2.099 %	16.094 %	4.650 %

TABLE IV: Near collision scenarios inside test dataset

	Average acceleration (m/s^2)	Uncomfortable scenarios (%)	Near collision (%)
I-80 medium congestion traffic			
Consensus cases			
Rule based	0.089	71.058	7.235
Imitation	0.132	57.325	7.087
PMP-DRL	0.239	37.481	7.142
Conflict cases			
Rule based	0.070	77.600	15.435
Imitation	0.082	73.766	15.396
PMP-DRL	0.254	37.330	15.869
US-101 medium congestion traffic			
Consensus cases			
Rule based	0.082	74.910	9.323
Imitation	0.087	73.245	9.271
PMP-DRL	0.282	37.553	9.081
Conflict cases			
Rule based	0.034	89.268	14.998
Imitation	0.036	88.678	14.982
PMP-DRL	0.283	37.474	14.728

TABLE V: Comparative results

models. The imitative model suffers from unseen data distribution. The PMP-DRL-based method decides more safe and more comfortable actions. As the average acceleration metric shows, it also moves faster through the traffic. A trade-off exists between near-collision scenarios and uncomfortable scenarios with average acceleration. For the comfort of passengers, ego vehicle can not change its decision very frequently. If some scenario changes very quickly, the ego vehicle must change its decisions abruptly. This abrupt change will make the ego vehicle safe; however, the comfortability of passengers will be reduced. Table V shows that the PMP-DRL method performs similarly to the imitative model for near-collision scenarios. It has been found that the PMP-DRL method takes such decisions where 7.142% and 15.869% of cases occur in near-collision scenarios for the 180 dataset. In the human-driven decisions, there are 7.132% and 16.094% cases; at least one vehicle was in the near collision region as given in Table IV. From this, we can infer that the DRL-PMP method makes decisions such that fewer near-collision scenarios happen during driving than human driving. The imitative model mimics actions that are only safe but uncomfortable. Hence, the imitative model performs poorly compared to PMP-DRL for comfortable scenarios. For comfortability, PMP-DRL gives 19.84% and 35.69% improvement for consensus cases and 36.69% and 51.20% improvement for conflict cases in comparison with the imitative model. Also, the average acceleration is much higher with PMP-DRL than with the imitative model. This implies that the ego vehicle can move smoothly without making too many jerks.

	Average acceleration (m/s^2)	Uncomfortable scenarios (%)	Near collision (%)
I-80 medium congestion traffic			
Consensus cases			
Imitation (P)	0.005	95.688	7.252
Imitation (PP)	0.086	71.847	7.230
PMP-DRL	0.239	37.481	7.142
Conflict cases			
Imitation (P)	0.042	86.281	15.460
Imitation (PP)	0.070	77.561	15.440
PMP-DRL	0.254	37.330	15.869
US-101 medium congestion traffic			
Consensus cases			
Imitation (P)	0.002	98.645	9.308
Imitation (PP)	0.079	75.829	9.322
PMP-DRL	0.282	37.553	9.081
Conflict cases			
Imitation (P)	0.013	95.930	14.978
Imitation (PP)	0.034	89.275	14.900
PMP-DRL	0.283	37.474	14.728

TABLE VI: Comparisons of the effectiveness of prediction

D. Ablation study

This section presents the importance of surrounding vehicles' future position prediction module in maneuver planning for AV. The results are presented with the same metrics defined earlier. The input context-aware social grid maps include the past, present, and predicted future context information around the ego vehicle. The different time steps in the contextual grid maps present information that can help take safe, efficient, and comfortable actions. Hence, in this study, three different models have been trained. One model(Imitation(P)) has been trained with only the current instant occupancy grid map. Another model (Imitation(PP)) uses all the 3 seconds of past and current occupancy maps for training. Finally, the proposed model (PMP-DRL) has been trained with predicted future POMs with past occupancy maps. The comparisons are shown in Table VI. The Table shows that the performance improved significantly using the predicted future information in the context-aware social grid maps. There is 34.37% and 38.276% improvement for consensus scenarios, 40.23% and 51.80% improvement for conflicting scenarios, for comfortable decision making. There is also a significant improvement in the average acceleration and near-collision scenarios when using future prediction.

IV. CONCLUSION

This paper presents a data-driven method for Predictive Maneuver Planning with Deep Reinforcement Learning (PMP-DRL) for safe and comfortable autonomous driving. The surrounding vehicles' past trajectories are encoded in an occupancy grid map. Occupancy grid maps are created with the predicted future positions of surrounding vehicles along with their uncertainty estimates. PMP-DRL shows better performance than rule-based and imitative models. The rule-based method looks for safety, not passengers' comfort. The imitative model suffers from uncomfortable decision-making as it tries to learn traffic rules broadly. The results show an improvement with DRL-PMP in near-collision scenarios and a significant improvement of 35.69% and 51.20% in comfortability compared to the imitative model. Also, we show how predictions

help in safe and comfortable maneuvering decision-making. There are 40.23% and 51.80% improvements in comfort while using future predictions for maneuver planning. The results clearly indicate the importance of the proposed prediction module in data-driven reinforcement learning over an imitative model.

REFERENCES

- [1] A. Bazzi, A. O. Berthet, C. Campolo, B. M. Masini, A. Molinaro, and A. Zanella, "On the design of sidelink for cellular v2x: A literature review and outlook for future," *IEEE Access*, vol. 9, pp. 97 953–97 980, 2021.
- [2] M. Bansal, A. Krizhevsky, and A. Ogale, "Chauffeurnet: Learning to drive by imitating the best and synthesizing the worst," *arXiv preprint arXiv:1812.03079*, 2018.
- [3] P. Wang, D. Liu, J. Chen, H. Li, and C.-Y. Chan, "Decision making for autonomous driving via augmented adversarial inverse reinforcement learning," in *2021 IEEE International Conference on Robotics and Automation (ICRA)*, 2021, pp. 1036–1042.
- [4] A. Dosovitskiy, G. Ros, F. Codevilla, A. Lopez, and V. Koltun, "Carla: An open urban driving simulator," in *Conference on robot learning*. PMLR, 2017, pp. 1–16.
- [5] A. Amini, T.-H. Wang, I. Gilitschenski, W. Schwarting, Z. Liu, S. Han, S. Karaman, and D. Rus, "Vista 2.0: An open, data-driven simulator for multimodal sensing and policy learning for autonomous vehicles," in *2022 International Conference on Robotics and Automation (ICRA)*, 2022, pp. 2419–2426.
- [6] N. Rhinehart, R. McAllister, and S. Levine, "Deep imitative models for flexible inference, planning, and control," in *International Conference on Learning Representations*, 2020.
- [7] F. Codevilla, M. Müller, A. López, V. Koltun, and A. Dosovitskiy, "End-to-end driving via conditional imitation learning," in *2018 IEEE International Conference on Robotics and Automation (ICRA)*, 2018, pp. 4693–4700.
- [8] P. Cai, S. Wang, Y. Sun, and M. Liu, "Probabilistic end-to-end vehicle navigation in complex dynamic environments with multimodal sensor fusion," *IEEE Robotics and Automation Letters*, vol. 5, no. 3, pp. 4218–4224, 2020.
- [9] W. Shu, K. Cai, and N. N. Xiong, "A short-term traffic flow prediction model based on an improved gate recurrent unit neural network," *IEEE Transactions on Intelligent Transportation Systems*, vol. 23, no. 9, pp. 16 654–16 665, 2022.
- [10] V. Katariya, M. Baharani, N. Morris, O. Shoghli, and H. Tabkhi, "Deeptrack: Lightweight deep learning for vehicle trajectory prediction in highways," *IEEE Transactions on Intelligent Transportation Systems*, vol. 23, no. 10, pp. 18 927–18 936, 2022.
- [11] B. Mersch, T. Höllen, K. Zhao, C. Stachniss, and R. Roscher, "Maneuver-based trajectory prediction for self-driving cars using spatio-temporal convolutional networks," in *2021 IEEE/RSJ International Conference on Intelligent Robots and Systems (IROS)*, 2021, pp. 4888–4895.
- [12] J. Chowdhury, S. Sundaram, N. Rao, and N. Sundararajan, "An efficient Deep Spatio-Temporal Context Aware decision Network (DST-CAN) for predictive manoeuvre planning," *arXiv preprint arXiv:2205.10092*, 2022.
- [13] J. Colyar and J. Halkias, "US highway 101 dataset," *Federal Highway Administration (FHWA), Tech. Rep. FHWA-HRT-07-030*, 2007.
- [14] J. Chen, B. Yuan, and M. Tomizuka, "Model-free deep reinforcement learning for urban autonomous driving," in *2019 IEEE Intelligent Transportation Systems Conference (ITSC)*. IEEE, 2019, pp. 2765–2771.
- [15] J. Chen, S. E. Li, and M. Tomizuka, "Interpretable end-to-end urban autonomous driving with latent deep reinforcement learning," *IEEE Transactions on Intelligent Transportation Systems*, vol. 23, no. 6, pp. 5068–5078, 2021.
- [16] F. Ye, X. Cheng, P. Wang, C.-Y. Chan, and J. Zhang, "Automated lane change strategy using proximal policy optimization-based deep reinforcement learning," in *2020 IEEE Intelligent Vehicles Symposium (IV)*. IEEE, 2020, pp. 1746–1752.
- [17] X. Tang, B. Huang, T. Liu, and X. Lin, "Highway decision-making and motion planning for autonomous driving via soft actor-critic," *IEEE Transactions on Vehicular Technology*, vol. 71, no. 5, pp. 4706–4717, 2022.
- [18] J. Schulman, F. Wolski, P. Dhariwal, A. Radford, and O. Klimov, "Proximal policy optimization algorithms," *arXiv preprint arXiv:1707.06347*, 2017.
- [19] T. Haarnoja, A. Zhou, P. Abbeel, and S. Levine, "Soft actor-critic: Off-policy maximum entropy deep reinforcement learning with a stochastic actor," in *Proceedings of the 35th International Conference on Machine Learning*, ser. Proceedings of Machine Learning Research, J. Dy and A. Krause, Eds., vol. 80. PMLR, 10–15 Jul 2018, pp. 1861–1870.
- [20] A. Alizadeh, M. Moghadam, Y. Bicer, N. K. Ure, U. Yavas, and C. Kurtulus, "Automated lane change decision making using deep reinforcement learning in dynamic and uncertain highway environment," in *2019 IEEE Intelligent Transportation Systems Conference (ITSC)*, 2019, pp. 1399–1404.
- [21] K. B. Naveed, Z. Qiao, and J. M. Dolan, "Trajectory planning for autonomous vehicles using hierarchical reinforcement learning," in *2021 IEEE International Intelligent Transportation Systems Conference (ITSC)*, 2021, pp. 601–606.
- [22] Z. Zhu and H. Zhao, "A survey of Deep RL and IL for autonomous driving policy learning," *IEEE Transactions on Intelligent Transportation Systems*, vol. 23, no. 9, pp. 14 043–14 065, 2022.
- [23] S. Levine, A. Kumar, G. Tucker, and J. Fu, "Offline reinforcement learning: Tutorial, review, and perspectives on open problems," *arXiv preprint arXiv:2005.01643*, 2020.
- [24] R. F. Prudencio, M. R. O. A. Maximo, and E. L. Colombini, "A survey on offline reinforcement learning: Taxonomy, review, and open problems," *IEEE Transactions on Neural Networks and Learning Systems*, pp. 1–0, 2023.
- [25] A. Amini, I. Gilitschenski, J. Phillips, J. Moseyko, R. Banerjee, S. Karaman, and D. Rus, "Learning robust control policies for end-to-end autonomous driving from data-driven simulation," *IEEE Robotics and Automation Letters*, vol. 5, no. 2, pp. 1143–1150, 2020.
- [26] P. Sastry, G. Santharam, and K. Unnikrishnan, "Memory neuron networks for identification and control of dynamical systems," *IEEE transactions on neural networks*, vol. 5, no. 2, pp. 306–319, 1994.
- [27] V. Kumar, O. S N, R. Ganguli, P. Sampath, and S. Suresh, "Identification of helicopter dynamics using recurrent neural networks and flight data," *JOURNAL OF THE AMERICAN HELICOPTER SOCIETY*, vol. 51, pp. 164–174, 04 2006.
- [28] H. Van Hasselt, A. Guez, and D. Silver, "Deep reinforcement learning with double q-learning," in *Proceedings of the AAAI conference on artificial intelligence*, vol. 30, no. 1, 2016.
- [29] N. Rao and S. Sundaram, "Spatio-temporal look-ahead trajectory prediction using memory neural network," in *2021 International Joint Conference on Neural Networks (IJCNN)*, 2021, pp. 1–8.
- [30] R. Song and B. Li, "Surrounding vehicles' lane change maneuver prediction and detection for intelligent vehicles: A comprehensive review," *IEEE Transactions on Intelligent Transportation Systems*, vol. 23, no. 7, pp. 6046–6062, 2022.